Mol Psychiatry. Author manuscript; available in PMC 2019 May 01.

Published in final edited form as:
Mol Psychiatry. 2018 November ; 23(11): 2209–2226. doi:10.1038/s41380-018-0046-0.

A novel role for CAMKIIβ in the regulation of cortical neuron migration: implications for neurodevelopmental disorders

Olivier Nicole[1,6], **Donald M. Bell**[2], **Thierry Leste-Lasserre**[3], **Hélène Doat**[3], **François Guillemot**[4], and **Emilie Pacary**[5,6,*]

[1]CNRS, UMR5293, Institut des Maladies Neurodégénératives, F-33000 Bordeaux, France

[2]Confocal and Image Analysis Facility, The Francis Crick Institute, 1 Midland Road, London NW1 1AT, UK

[3]Transcriptome Facility, INSERM U1215, Neurocentre Magendie, F-33000 Bordeaux, France

[4]The Francis Crick Institute, 1 Midland Road, London NW1 1AT, UK

[5]INSERM U1215, Neurocentre Magendie, F-33000 Bordeaux, France

[6]Université de Bordeaux, F-33000 Bordeaux, France

Abstract

Perturbation of *CaMKIIβ* expression has been associated with multiple neuropsychiatric diseases, highlighting *CaMKIIβ* as a gene of interest. Yet, in contrast to CaMKIIα, the specific functions of CaMKIIβ in the brain remain poorly explored. Here, we reveal a novel function for this CaMKII isoform *in vivo* during neuronal development. By using *in utero* electroporation, we show that CaMKIIβ is an important regulator of radial migration of projection neurons during cerebral cortex development. Knockdown of *CaMKIIβ* causes accelerated migration of nascent pyramidal neurons, whereas overexpression of CaMKIIβ inhibits migration, demonstrating that precise regulation of CaMKIIβ expression is required for correct neuronal migration. More precisely, CaMKIIβ controls the multipolar-bipolar transition in the intermediate zone and locomotion in the cortical plate through its actin-binding and -bundling activities. In addition, our data indicate that a fine-tuned balance between CaMKIIβ and cofilin activities is necessary to ensure proper migration of cortical neurons. Thus, our findings define a novel isoform-specific function for CaMKIIβ, demonstrating that CaMKIIβ has a major biological function in the developing brain.

Introduction

During brain development, neurons migrate extensively after their birth to reach their final destination, where they establish connections with other neurons and contribute to circuit

*Correspondence: emilie.pacary@inserm.fr.

Author Contributions

E.P. and O.N. designed and carried out experiments. E.P. wrote the manuscript. D.B. and F.G helped with live imaging experiments. T.LL. and H.D. performed PCR analyses. All authors discussed results from experiments and commented on the manuscript.

Conflict of Interest

The authors declare no conflict of interest.

Europe PMC Funders Author Manuscripts

formation. Several psychiatric and neurological diseases are considered as neurodevelopmental disorders because they result from abnormal neuronal development, especially from defects in neuronal migration, thereby underscoring the importance of this process for normal brain function 1–3. Unraveling the complexities of neuronal migration is thus essential to our understanding of both normal cortical development and neurodevelopmental disorders.

In the developing cerebral cortex, newborn pyramidal neurons undergo radial migration to reach their correct position within the cortical plate (CP) 4. Radial migration is a multiphasic process starting with the detachment of newly born neurons from the apical surface of the germinal ventricular zone (VZ). Nascent neurons then move to the intermediate zone (IZ) where they acquire a multipolar shape 5. Thereafter neurons become bipolar, extending a leading process towards the pial surface and a trailing process in the opposite direction. Upon multi to bipolar transition, neurons establish dynamic contacts with radial glia fibers and subsequently use them as a scaffold to migrate to the upper part of the CP using a mode of migration called locomotion 6. This movement is characterized by repetitive cycles of synchronized steps - formation of a cytoplasmic dilatation in the proximal region of the leading process, movement of the centrosome towards the swelling and translocation of the nucleus towards the centrosome - conferring a saltatory advancement to locomoting neurons 7, 8. Finally, once neurons approach their final location, they change again their mode of migration from locomotion to terminal translocation and finally settle in a specific cortical layer 9.

The locomotion mode of neuronal migration covers the largest part of the neuronal journey in the developing cerebral cortex. This process requires a dynamic cellular remodeling which largely depends on the coordinated activity of the actin and microtubule cytoskeletons 6, 10–12. More precisely, the coordination between the centrosome and the nucleus depends on the microtubule network that couples these two organelles, including the perinuclear cage that surrounds the nucleus 13. Actin filaments, which are enriched in the proximal portion of the leading process, are essential for the formation of the proximal cytoplasmic dilation in the leading process 14 and also provide a major driving force for the coordinated movement of the centrosome and soma during neuronal migration 15, 16. The actomyosin-based contraction at the cell rear might also provide additional forces to promote forward nuclear movement 16. While the cytoskeleton is clearly involved in the dynamic changes occurring during locomotion but also during the multipolar-bipolar transition 17, it is still largely unknown how cytoskeleton components are regulated and coordinated during these processes. Thus, identification of new cytoskeleton regulators is fundamental to shed light on the molecular mechanisms responsible for proper cortical neuron migration.

The calcium/calmodulin-dependent protein kinase II (CaMKII) is a predominant protein in the brain, accounting for 1-2% of total brain proteins 18. Because of this abundance and as major player in Ca^{2+} signaling, CaMKII represents a critical link between the external environment and cellular responses in neurons. There are four isoforms of CaMKII (α, β, γ, δ) encoded by separate genes. CaMKII exists as a holoenzyme composed of twelve subunits, which form a complex through their association domains. Brain CaMKII predominantly consists of the α and β isoforms, which form heteromeric or homomeric complexes 19.

While the brain functions of CaMKIIα have been extensively studied 20, 21, the isoform-specific functions of CaMKIIβ are less characterized and remain largely undefined *in vivo*. Interestingly, this isoform is expressed in the embryonic cerebral cortex whereas the α isoform is absent 22, 23, interacts directly with the actin cytoskeleton 24 and its expression is modified in neuropsychiatric illnesses including schizophrenia 25, 26. In view of these data suggesting that CaMKIIβ might have unique and important roles in cortical development, we have investigated its contribution to cerebral corticogenesis. Importantly, we have discovered a key role for this isoform in regulating radial migration of projection neurons. In particular, we demonstrate that CaMKIIβ is a critical element not only for the transition between the multipolar and the bipolar stage but also for the saltatory movement of locomoting neurons. This activity is dependent on its actin-binding and bundling properties.

Materials and Methods

Animals

Time pregnant CD1 females were housed, bred, and treated according to the European directive 2010/63/EU, French laws on animal experimentation and according to the guidelines approved by the Home Office under the Animal (Scientific Procedures) Act 1986.

Plasmid constructs

CaMKIIβ#1 shRNA and *CaMKIIβ#2* shRNA were obtained by cloning the following sequences into the short hairpin RNA vector, pCA-b-EGFPm5 silencer 3 (generous gift from Dr Vermeren): *CaMKIIβ#1*, 5’-GTCCGACGCTGTGTCAAGC-3’ 27; *CaMKIIβ#2*, 5’-GAGTATGCAGCCAAGATCA-3’ 28 adapted to mouse sequence. Control (ctrl) shRNA construct was generated by cloning into pCA-b-EGFPm5 silencer 3 a 19 bp scrambled sequence (5’-TACGCGCATAAGATTAGGG-3’) with no significant homology to any known gene sequence from mouse or human as previously described 29.

CaMKIIβ cloned into the pEGFP-C1 vector (with a CMV promoter) was a kind gift from Dr Paul De Koninck, CaMKIIβ-ΔFABD, CaMKIIβ-Δasso, CaMKIIβ-K43R and CaMKIIβ-ΔCTS cloned into the pEGFP-C1 vector from Dr Azad Bonni, CaMKIIβ-All A and CaMKIIβ-All D cloned into the pEGFP-C1 vector from Dr Yasunori Hayashi, pcDNA-cofilinS3D, pcDNA-cofilinS3A and pcDNA-cofilinWT from Iryna M. Ethell and pCIG2-Centrin2-Venus construct from Dr. Mary E. Hatten.

CaMKIIβ, CaMKIIβ-ΔFABD, CaMKIIβ-Δasso, CaMKIIβ-K43R, CaMKIIβ-ΔCTS, CaMKIIβ-All A and CaMKIIβ-All D were cloned by PCR using pEGFP-C1 constructs as template and then inserted into the XhoI/EcoRI sites of the pCIG2 vector to generate pCIG-CaMKIIβ and the different mutants.

To generate expression constructs harboring silent point mutations in the sequence recognized by *CaMKIIβ#1* shRNA (marked CaMKIIβ*), site-directed mutagenesis was performed using QuickChange II Site-Directed Mutagenesis Kit (Stratagene) on pEGFPC1-CaMKIIβ plasmid or mutant constructs using the following primers: forward, 5’-CTTTCTCTGTGGTGCGACGGTGTGTGAAGCTCTGTACCG-3’ and reverse, 5’-

CGGTACAGAGCTTCACACACCGTCGCACCACAGAGAAAG-3'. The underlined nucleotide residues identify silent mutations on nt84(C→G), nt90(C→G) and nt96(C→G) of the CaMKIIβ cDNA sequence.

CaMKIIβ was cloned by PCR into the XhoI site of the dephosphorylated pNeuroD1-IRES-GFP expression plasmid to generate pND-CaMKIIβ.

All of the above mentioned constructs were fully sequenced verified before their use in experiments.

In utero electroporation and tissue processing

In utero electroporation of the cerebral cortex was performed at E14.5 as previously described 30, 31. A concentration of 1 μg/μl was used for each construct. At the desired time point after electroporation, pregnant mice were sacrificed by neck dislocation and embryos were processed for tissue analyses. Embryonic brains were fixed in 4% paraformaldehyde (PFA) overnight and then placed in 20% sucrose/PBS overnight. Brains were then embedded in OCT Compound (VWR International) and frozen before sectioning using a cryostat (14 μm). For analysis at P14 and 8 weeks, brains were removed from anesthetized pups subjected to intracardiac perfusion of PBS followed by 4% PFA in PBS. Brains were then post-fixed in 4% PFA and cut with a vibratome (40μm).

For migration analysis, the different subregions of the cerebral cortex (VZ/SVZ, IZ and CP) were identified based on cell density and visualized with TOTO-3 iodide nuclear staining (Invitrogen) 30. Images were acquired with a confocal microscope (Leica SP5 or SP8). For migration experiments, at least six sections were analyzed for each condition from at least three embryos or pups from two or three litters obtained in parallel experiments. Cell counts were performed using MetaMorph software.

For morphometrical analysis, dendrites of electroporated neurons were traced using a 100X objective and a semiautomatic neuron tracing system (Neurolucida; MicroBrightField).

Leading process width was measured by drawing a transversal line at the portion of the leading process adjacent to the nucleus with ImageJ 32 as previously described 33. For this analysis, cells exhibiting a nucleus with a round shape were selected.

Ex vivo cortical electroporation and live imaging

Ex vivo electroporation and live imaging were performed as previously described 29, 30. *Ex vivo* electroporation was performed on injected mouse embryos' heads similarly to *in vivo* electroporation. The electrical parameters were the following: 50V, 50 msec length, 5 pulses, 1 sec interval. Following electroporation, brains were dissected in L15 (PAA Laboratories) and transferred into liquid 3% low melting agarose (Sigma) and incubated on ice. Embedded brains were cut coronally (300 μm) with a vibratome (Leica), and slices were transferred onto sterilized culture plate inserts (0.4-μm pore size; Millicell-CM, Millipore) and cultivated in complete Neurobasal containing Neurobasal medium (Gibco) supplemented with 1% B27, 1% N2, 1% glutamine, 1% penicillin/streptomycin and 1% fungizone.

Thirty hours after ex vivo electroporation, GFP was imaged in live brain slices using 900nm multiphoton excitation (Spectraphysics MaiTai DeepSee) with a Leica SP5 confocal scanner on a DM6000 CFS upright microscope. A 10x,0.4NA (dry) objective was used and reflected excitation collected with a non descanned PMT through a 525/50 filter (Semrock).

Movies were analysed using the Fiji software 34. Three dimensional sample drift over time was corrected with the Correct 3D drift plug-in and cell movement was analysed using the Manual Tracking plug-in.

Immunostaining

After washing in PBS, sections or fixed cells (with PFA 4%, 10 min at room temperature) were treated with PBS - 0.01% Triton X100 - 10% serum for 30 min. They were then incubated overnight at 4°C with the following primary antibodies diluted in the blocking buffer: rabbit anti-CaMKIIβ (1/300; Abcam, ab34703), mouse anti-CaMKIIδ (1/50, Santa Cruz, sc-100362), mouse anti-CaMKIIγ (1/50, Santa Cruz, sc-517278), rabbit anti-Cux1 (1/50; Santa Cruz, sc-13024), chicken anti-GFP (1/1000; Abcam, ab13970), mouse anti-Ki67 (1/50; BD Pharmingen™, 550609), mouse anti-NeuN (1/500; Millipore, MAB377), rabbit anti-pHH3 (1/200; Upstate, 06-570), rabbit anti-Tbr2 (1/500; Abcam, ab23345), mouse anti-Tuj1 (1/200; Covance, MMS-435P). Sections were then incubated with appropriate fluorescent secondary antibodies. For Cux1 and NeuN immunostainings, a step of antigen retrieval with citrate was performed before the step of blocking (sodium citrate pH=6 for 15 min at 90°C).

F-actin filaments were visualized using rhodamine-labelled phalloidin (Sigma). After fixation, sections or cells were permeabilized 10 min with 0.1% Triton X100 - PBS, incubated with rhodamine-labelled phalloidin diluted in PBS (0.2 μg/ml) for 40 min and washed several times in PBS.

RNA in situ hybridization

Embryonic brains were dissected in 1X PBS and fixed overnight in 4% PFA/1× PBS at 4°C. Fixed samples were cryoprotected overnight in 20% sucrose/1× PBS at 4°C, mounted in OCT Compound and sectioned coronally with a cryostat (14μm). Nonradioactive RNA in situ hybridizations on frozen brain sections were performed with digoxigenin-labelled riboprobes as described previously 35. The RNA sens and antisense probes for *CaMKIIβ* were kindly provided by Dr Franck Oury 36.

Cell culture

Mouse embryonic teratocarcinoma P19 cells were cultured in high glucose Dulbecco's modified eagle medium (DMEM) (Sigma) supplemented with 10% foetal bovine serum, 2mM glutamine and 1% penicillin/streptomycin. Cells were plated in 24-well plates and incubated at 37°C under 5% CO_2 atmosphere. One day after plating, P19 cells were transfected with Lipofectamine 2000 reagent according to the manufacturer's protocol (Invitrogen). Twenty-four hours post-transfection, cells were collected for RNA or protein extraction.

Primary cortical neuron cultures were prepared from E13.5 or E14.5 mouse cortices. Cortices were dissected in Hepes 0.1M and then incubated for 15 min in trysin-EDTA (0.125%). After 2 washings in Hepes 0.1M, tissues were either dissociated in Optimem containing Lipofectamine and DNA (for transfection) or dissociated in Neurobasal medium (Gibco) supplemented with 2% B27, 1% N2, 2mM glutamine and 1% penicillin/streptomycin (for F-actin precipitation). Dissociated cortical cells were seeded on poly-D-lysine (25 μg/ml, Sigma) coated wells and cultured in complete Neurobasal medium for 4 days or 5 days.

F-actin precipitation

F-actin was isolated from cerebral cortices (E17.5) or neuronal cell cultures (E14+5DIV) after modification of a published protocol 37. Four cortices for each condition were dissected and transferred into 1 ml of homogenization buffer (100 mM Na_2HPO4 – 100 mM NaH_2PO4 at pH 7.2, 2 mM ATP, 2 mM $MgCl_2$, 0.1% Triton X-100) containing phosphatase and protease inhibitor cocktails (Sigma). For analysis on cultures, 16 wells of 24-well plates were pooled for each condition. When needed, cells were incubated for 10 min with 10 μM of the calcium ionophore A23187 (Tocris) before the lysis. Neurons were then lysed and homogenized, like tissues, at 4°C into 1 ml of homogenization buffer by pipetting up and down using a 18G needle. Biotinylated phalloidin (1 unit for each condition, Invitrogen) was then added to homogenates and incubated under rotation for 1 h at room temperature. In parallel, streptavidin-coated magnetic beads (50μl for each condition; Invitrogen) were blocked for 30 min in PBS (Sigma) with 5% bovine serum albumine (Sigma), washed and added to homogenates with biotinylated phallodin for 1 h at room temperature. The precipitated material was then washed five times with homogenization buffer, resuspended in 1X laemmli sample buffer (Bio-Rad) and analyzed by western blotting using primary antibodies against actin and CaMKIIβ according to the protocol described below.

Measurement of G/F-actin ratio by Triton X-100 fractionation

The measurement of monomeric (Triton soluble) and polymerized (Triton insoluble) actin in transfected P19 cells was performed as previously described 38 with minor modifications. Briefly, cells were gently washed with a cytoskeleton stabilization buffer containing 0.1 M MES (pH 6.75), 1 mM MgSO4, 2 mM EGTA, 0.1 mM EDTA, 4 M glycerol. Cells were then incubated with the cytoskeleton stabilization buffer supplemented with 0.1% Triton X-100 and protease inhibitors (Sigma) for 6 min at 37°C. The supernatant containing G-actin was collected and centrifuged at 10 000 g for 2 min at 4°C to remove debris. Extraction of the Triton insoluble fraction remaining on the culture plate was performed in lysis buffer containing 25 mM Tris (pH 6.8), 0.5% SDS and supplemented with protease inhibitors. Cells were scraped off and incubated in the lysis buffer for 30 min on ice to extract F-actin. Actin levels were quantified by immunoblot using a rabbit anti-actin antibody (1/2000; Sigma, A2066). For each condition we pooled four wells of a 24-well plate. Densitometry was performed using Odyssey software (LI-COR).

Protein extraction

Cerebral cortices were dissected and dissociated using a 18G needle in 100 μl of a solution containing 20 mM HEPES, 0.15 mM NaCl, 1% Triton X100, 1% deoxycholic acid, 1% SDS

(pH 7.5) and supplemented with phosphatase and protease inhibitor cocktails. Similar buffer was used to extract proteins from cells. After incubation for 1 h at 4°C, samples were centrifuged at 10000 g for 15 min. Supernatant was isolated and used as total protein extracts. Protein amounts were quantified using the Bradford's protein assay (Bio-Rad).

Western blotting

Electrophoresis was performed on precast 4-15% polyacrylamide Tris-Glycine gels (Bio-Rad). Protein levels were normalized to 50 μg of protein per sample and resuspended with 4X laemmli sample buffer (Bio-Rad) before boiling (5 min at 95°C). Then, proteins were transferred onto a polyvinylidenedifluoride (PVDF) membrane (Bio-Rad). Membranes were blocked with Tris-Tween Buffered solution (TTBS: 10 mM Tris, 200 mM NaCl, 0.05% Tween 20, pH 7.4) containing 5% non-fat dry milk for 1 h at room temperature. For F-actin precipitation studies, blots were then incubated overnight at 4°C with a mouse anti-CaMKII beta antibody (0,5μg/mL; Thermofisher, 139800) and a rabbit anti-actin antibody (1/2000; Sigma, A2066). For variant expression analysis, blots were incubated with a rabbit anti-CaMKIIβ (1/1000; Abcam, ab34703). Primary antibodies were probed with a IRDye 800CW goat anti-rabbit IgG together with a IRDye 680RD goat-anti mouse IgG (Li-Cor Biosciences) during 1 h incubation at room temperature. After 3 washes with TTBS and one with PBS, membrane was scanned using the automated infrared imaging system Odyssey (Li-Cor Biosciences) according to manufacturer's instructions.

Quantitative real-time PCR (qPCR)

Cell and tissue samples were homogenized in Tri-reagent (Euromedex) and RNA was isolated using a standard chloroform/isopropanol protocol. RNA was processed and analyzed following an adaptation of published methods 39. cDNA was synthesized from 2 μg of total RNA using RevertAid Premium Reverse Transcriptase (Fisher Scientific) and primed with oligo-dT primers (Fisher Scientific) and random primers (Fisher Scientific). qPCR was performed using a LightCycler® 480 Real-Time PCR System (Roche). qPCR reactions were done in duplicate for each sample, using transcript-specific primers (Table 1), cDNA and LightCycler 480 SYBR Green I Master mix (Roche) in a final volume of 10 μl. PCR data were exported and analyzed in the GEASE software (Gene Expression Analysis Software Environment) developed in the Neurocentre Magendie (https://bioinfo.neurocentre-magendie.fr/outils/GEASE/). For the determination of the reference genes, the GeNorm method was used 40. Relative expression analysis was corrected for PCR efficiency and normalized against two reference genes. The relative level of expression was calculated using the comparative (2-ΔΔCT) method 40.

Statistical analysis

Statistical analyses were performed using the GraphPad Prism software. No statistical methods were used to predetermine sample sizes, but our sample sizes are similar to those generally employed in the field. Molecular and biochemical analyses were performed using a minimum of three biological replicates per condition. Results are presented as mean ± s.e.m. The statistical test used for each experiment as well as sample size (n) are described in the corresponding figure legend.

Results

CaMKIIβ is expressed in post-mitotic cortical neurons and interacts with F-actin

We began this study by examining the expression of CaMKIIβ in the mouse developing cerebral cortex. We first showed by real-time PCR that *CaMKIIβ* expression increases significantly between E12.5 and postnatal day 0 (P0) (Figure 1a and Supplementary Figure 1b) whereas *CaMKIIα* transcripts are poorly expressed until birth (Supplementary Figure 1a). By RNA *in situ* hybridization on coronal brain sections, we then found that *CaMKIIβ* transcripts are detected mainly in the CP at different developmental stages (Figure 1b and Supplementary Figures 1d-e) and uniformly along the rostrocaudal axis (Supplementary Figure 1c). Immunostainings performed on E17.5 brains showed that CaMKIIβ is expressed in post-mitotic neurons, as identified by staining with the neuron-specific β-tubulin III marker Tuj1 (Figure 1c), in the upper part of the intermediate zone (IZ) and in the CP. Stainings also indicate that CaMKIIβ is expressed in multipolar and locomoting neurons (Supplementary Figures 1f and g). The four splice variants of CaMKIIβ (CaMKIIβ, β', βe, β'e) are expressed in the developing cerebral cortex (Figure 1d and Supplementary Figures 1h-k) and their protein levels increase significantly between E14.5 and P0 (Figure 1d). In addition CaMKIIβ interacts with filamentous-actin (F-actin) in nascent cortical neurons (Figures 1e-h), suggesting altogether that CaMKIIβ might play a role in cytoskeletal remodeling in radially migrating cortical neurons.

CaMKIIβ knockdown promotes radial migration of cortical neurons

To determine whether CaMKIIβ regulates radial migration of projection neurons, we used an acute loss-of-function approach by RNA interference. We designed two shRNAs that efficiently knocked down *CaMKIIβ* expression by targeting distinct regions of *CaMKIIβ* mRNA (Supplementary Figures 2 and 3b). Importantly, *CaMKIIβ* silencing in cortical neurons had no impact on the expression of the two other isoforms expressed in the embryonic brain 22, CaMKIIδ and CaMKIIγ (Supplementary Figure 3). We then introduced the two *CaMKIIβ* shRNAs together with EGFP expressed from the same construct by *in utero* electroporation in the cerebral cortex at E14.5. Electroporation of *CaMKIIβ* shRNA in the cortex did not induce cell death or defects in radial glia processes and did not alter neural progenitor proliferation as well as neuronal output (Supplementary Figure 4 and data not shown). However, three days after electroporation (E17.5), the distribution of electroporated cells in the different zones of the cortex was quantified and this analysis revealed that *CaMKIIβ* silencing caused an acceleration of migration into the CP (Figures 2a and b). Indeed almost 60% of cells electroporated with *CaMKIIβ#1 shRNA* at E14 already entered the CP after 3 days, in contrast to 51% in control condition (Figure 2b). In addition, most of the cells in the CP reached the upper part of this region (uCP) after *CaMKIIβ* knockdown (26.8 ± 1.9% of *CaMKIIβ#1* shRNA-electroporated cells compared with 18.5 ± 1.6% of control shRNA-electroporated cells) (Figure 2b). There was no significant difference in the VZ/SVZ and the morphology of radially migrating neurons was unaffected by *CaMKIIβ* depletion neither in the CP nor in the IZ (Supplementary Figure 5a).

To confirm our observations in fixed sections, we performed live imaging experiments to track migration of neurons expressing control or *CaMKIIβ#1* shRNA, the most efficient and

specific *CaMKIIβ* shRNA (Supplementary Figures 2a and 3b). shRNAs were introduced by *ex vivo* electroporation into the developing cortex at E14.5, brain sections were prepared and imaged 30 hours later. In accordance with our previous results, we found that *CaMKIIβ*-deficient cells moved faster in the CP (Supplementary Movie 1) with a mean speed value of 19.6 ± 1.1 μm/hr compared to 13.3 ± 1.1 μm/hr in control cells (Figures 2c and d). We then analyzed in more details the migration profiles of these neurons that had adopted a bipolar shape and were migrating in the CP (Supplementary Figures 5b-g). A saltatory step was defined as any increase in speed surrounded on both sides by periods of zero speed (= pauses) as previously described 41. Our quantifications indicated that *CaMKIIβ* silencing reduced significantly the number of pauses (Supplementary Figure 5f) and the number of saltatory steps per hour (Supplementary Figure 5b). In addition, the duration of the saltatory step in this condition was increased as well as the speed and the distance travelled during this forward movement (Supplementary Figures 5c-e). The reduction in pausing frequency after *CaMKIIβ* knockdown together with the increased migration speed during the salutatory steps might explain the accelerated migration of neurons in this condition. Moreover, as a result of this pause reduction, the movement of *CaMKIIβ*-silenced cells towards the upper part of the CP appeared less saltatory (Supplementary Movies 2-3) but instead more continuous compared to control cells (Supplementary Movies 4 and 8) 29. We also analyzed the dynamic multipolar-bipolar transition of cortical neurons and found that *CaMKIIβ* knockdown favors this process (Figure 2e). Accordingly, 2 days after the electroporation, when most electroporated cells are located in the VZ/SVZ and in the IZ in control condition, we observed that *CaMKIIβ* silencing increased significantly the ratio of GFP+ cells in the CP, in particular in the lower CP (lCP) and median CP (mCP) (Supplementary Figures 5h and i). Therefore, when *CaMKIIβ* is silenced, neurons quickly leave the IZ after the multipolar-bipolar transition to reach the CP. This might explain why the proportion of multipolar/bipolar cells is not significantly affected after *CaMKIIβ* knockdown (Supplementary Figure 5a). *CaMKIIβ* silencing then promotes the locomotion of cortical neurons in the CP which also contributes to the acceleration of migration.

Analyses conducted at postnatal day 14 (P14), showed that *CaMKIIβ*-depleted neurons finally reached their terminal destination properly (Supplementary Figures 5j and k) but exhibited longer, more branched dendrites compared to control neurons (Supplementary Figures 6a-d), an effect already described in primary cerebral cortical neurons 27. Changes in the dendritic arborization of *CaMKIIβ*-silenced projection neurons were still observed in adult mice (Supplementary Figures 6e-h) indicating that *CaMKIIβ* knockdown during embryonic development impacts neuronal morphology in the adult brain. Thus, *CaMKIIβ* silencing in nascent cortical neurons perturbs different aspects of corticogenesis and has a long-term impact on the brain.

CaMKIIβ overexpression alters migration of cortical projection neurons

Because *CaMKIIβ* knockdown promotes cortical neuron migration, we investigated whether conversely overexpression of *CaMKIIβ* impairs this process. *CaMKIIβ* was overexpressed at high level (pCIG-CaMKIIβ) in E14.5 cerebral cortices by *in utero* electroporation together with a plasmid encoding GFP (Supplementary Figures 7 and 8a). Importantly, CaMKIIβ overexpression did not modify CaMKIIδ and CaMKIIγ expressions in cortical neurons

(Supplementary Figure 8). Examination of the electroporated brains at E17.5 revealed a marked defect in the migration of *CaMKIIβ* expressing cells compared with control cells (Figure 3a). Indeed *CaMKIIβ* expression resulted in a significant decrease in the fraction of cells reaching the CP (44.1 ± 3.2% of *CaMKIIβ* electroporated cells compared with 55.9 ± 1.0% of control cells) and particularly the upper part of the CP (9.1 ± 0.9% versus 25.6 ± 1.9%) whereas the fraction in the IZ was concomitantly increased (36.9 ± 3.0% versus 27.2 ± 1.6%) (Figure 3b). Additional studies with *CaMKIIβ* expression at lower levels with CMV or NeuroD promoters indicated that the extent of the migration defects correlates with the degree of *CaMKIIβ* overexpression (Supplementary Figures 9a and b). A closer look at the cortical wall revealed that *CaMKIIβ* overexpression increased the proportion of multipolar cells in the IZ at the expense of uni/bipolar cells while migrating neurons in the CP did not show grossly affected morphology (Figure 3c). These observations were corroborated by our live imaging studies indicating that *CaMKIIβ* expression in cortical cells impaired the multipolar-bipolar conversion (Figure 3d) and reduced migration speed in the CP (8.6 ± 0.6 μm/hr versus 11.5 ± 0.9 μm/hr) (Supplementary Movie 5, Figures 3e and f) Moreover *CaMKIIβ* overexpression reduced the distance travelled during a saltatory step (Supplementary Figure 9e), an effect that can be visualized in movies of isolated *CaMKIIβ* expressing cells (Supplementary Movies 6-8).

We then investigated whether the early overexpression of *CaMKIIβ* affects neuronal positioning at postnatal stage. At P14, we quantified the proportion of electroporated cells in 10 arbitrarily defined layers of the same size along the cortex. While many *CaMKIIβ* expressing cells finally reached their terminal position in bins 7 and 8, there was still a significant fraction of cells packed in lower bins, suggesting that *CaMKIIβ* levels critically determine the migratory behavior of cortical cells (Figures 3g and h). However the neurons trapped in deep layers expressed the upper-layer marker Cux1 indicating that *CaMKIIβ* expression impairs migration but not laminar specification (Supplementary Figure 9i and j).

The proliferation of cortical progenitors, the rate of cell death and the organization of the radial glia scaffold remained unperturbed, indicating that *CaMKIIβ* overexpression interferes specifically and cell autonomously with neuronal migration (Supplementary Figures 9k and l; data not shown). Altogether, the aforementioned results demonstrate that normal CaMKIIβ levels are required for correct radial migration in the embryonic cerebral cortex.

CaMKIIβ activity in locomoting neurons requires its F-actin-binding and multimerization domains

The identification of a novel role for CaMKIIβ in the control of neuronal migration led us to determine the molecular basis of CaMKIIβ function in migrating cortical neurons. To this goal, we asked whether mutations in specific regions of CaMKIIβ could abolish its deleterious effect on radial migration. First, to test the contribution of kinase activity in the regulation of neuronal migration, we used a catalytically inactive mutant of CaMKIIβ (K43R) (Supplementary Figure 10a). Overexpression of this mutated form of CaMKIIβ impaired radial migration similarly to wild-type CaMKIIβ suggesting that the migration defects induced by *CaMKIIβ* overexpression do not involve the catalytic activity of the

kinase (Figures 4a and b). In contrast to CaMKIIα, CaMKIIβ harbors, within the N-terminal part of the variable region, an F-actin binding domain (FABD) (Supplementary Figure 10a), which is important for recruiting CaMKII to F-actin 24. Moreover, CaMKIIβ is capable of bundling F-actin thanks to its actin-binding and association domains 28 (Supplementary Figure 10a). This bundling feature is achieved by the CaMKII oligomers binding to multiple actin filaments. Interestingly, the removal of the FABD in CaMKIIβ (CaMKIIβ-ΔFABD) or the association domain (CaMKIIβ-Δasso) abrogated the capacity of CaMKIIβ to impair migration (Figures 4a and b) suggesting that the migration defects are due to the actin-bundling activity of CaMKIIβ. We also studied the contribution of the centrosomal targeting sequence (CTS) within the variable region of CaMKIIβ. This CTS endows CaMKIIβ with the ability to localize to the centrosome 27. We overexpressed a mutant in which the CTS was deleted (CaMKIIβ-ΔCTS, Supplementary Figure 10a) and found that this mutated form of CaMKIIβ impaired radial migration similarly to wild-type CaMKIIβ (Figures 4a and b) suggesting that the migration defects induced by CaMKIIβ overexpression do not involve the localization of CaMKIIβ to the centrosome.

To further establish the contribution of the FABD and association domains in the regulation of neuronal migration, we performed rescue of *CaMKIIβ* knockdown neurons by expression of wild-type or mutated CaMKIIβ, refractory to silencing by *CaMKIIβ#1* shRNA (marked CaMKIIβ*) (Supplementary Figure 10b). As expected, the abnormal migratory behavior of *CaMKIIβ*-silenced neurons was fully corrected by co-delivery of CaMKIIβ* (Supplementary Figures 10c and d), thus demonstrating the specificity of the phenotype. In accordance with our previous experiments, CaMKIIβ*-K43R and CaMKIIβ*-ΔCTS rescued the migration of *CaMKIIβ*-silenced cortical cells, further suggesting that CaMKIIβ action in the cortex is independent of its kinase activity and its localization to the centrosome. Inversely, CaMKIIβ*-ΔFABD and CaMKIIβ*-Δasso were completely inactive in the *CaMKIIβ* knockdown rescue assay (Supplementary Figures 10c and d), thus confirming that the actin binding and association domains of CaMKIIβ are critical for its action in the regulation of cortical neuron migration.

Real-time imaging confirmed our previous observations by showing that CaMKIIβ-ΔFABD and CaMKIIβ-Δasso abolished the capacity of CaMKIIβ to impair the multipolar-bipolar conversion (Figure 4c) and to reduce the migration speed in the CP (Figure 4d), where neurons migrate using locomotion. A key feature of this mode of migration is the coordinated movement between the nucleus and the centrosome. To determine whether CaMKIIβ regulates this process, we co-electroporated a centrin–Venus construct together with *CaMKIIβ* and measured the distance between the centrosome and the tip of the nucleus (Figure 4e) as an indication of centrosome-nucleus coupling. As shown in Figure 4f, this distance was increased in *CaMKIIβ*-expressing neurons (3.3 ± 0.4 μm) compared with control neurons (2.0 ± 0.3 μm), suggesting that CaMKIIβ expression affects radial migration by perturbing the step of locomotion. This was further supported by the increased thickness of the leading process in *CaMKIIβ*-expressing neurons (2.35 ± 0.15 μm versus 1.88 ± 0.12 μm in control cells) (Figure 4g), another phenotype associated with defective nucleus-centrosome coupling 33, 42. Interestingly these two defects disappeared when CaMKIIβ was unable to bind and bundle F-actin (Figures 4e-g). Altogether, these data show that CaMKIIβ overexpression alters nucleus-centrosome coupling in locomoting neurons and the

actin-bundling activity of CaMKIIβ is responsible for these migration defects. CaMKIIβ might thus control locomotion of projection neurons by acting on the actin filaments, which are particularly enriched in the proximal portion of the leading process.

To determine whether CaMKIIβ acts on dendrites via similar domains, we then implemented a new set of rescue experiments and analyzed the dendritic arborization of electroporated neurons at P14. In a previous study performed in cerebellar neurons 27, it was shown that the CTS of CaMKIIβ is required for CaMKIIβ-regulation of dendrite patterning. We thus performed the rescue experiments with the CaMKIIβ*-ΔCTS mutant as well as with the CaMKIIβ*-ΔFABD and CaMKIIβ*-Δasso mutants. As shown in Supplementary Figure 11 and in accordance with the literature, CaMKIIβ*-ΔCTS failed to rescue the dendritic defects induced by *CaMKIIβ* knockdown indicating that the CTS is necessary for CaMKIIβ activity on dendrites. Inversely, CaMKIIβ*-ΔFABD and CaMKIIβ*-Δasso fully compensated the dendrite defects induced by *CaMKIIβ* silencing demonstrating that the FABD and the association domain in CaMKIIβ are not involved in this process. Taken together these data show that CaMKIIβ regulates neuronal migration and dendrite patterning in the developing cerebral cortex through different domains.

Autophosphorylation sites within the F-actin binding domain control CaMKIIβ action in migrating neurons

Importantly, the binding of CaMKIIβ to the actin cytoskeleton has been shown to be controlled by Ca^{2+} signaling 23, 43. In accordance with the literature, we confirmed that in nascent cortical neurons the interaction of CaMKIIβ with F-actin is almost completely lost after an increase in intracellular Ca^{2+} concentration (Figure 5a). A recent report further described the mechanisms involved in spines and demonstrated that the activation of CaMKII by Ca^{2+} influx results in autophosphorylation of the FABD, detaching CaMKII from F-actin 44. In this study, a phosphomimetic All D mutant, where all S and T residues within the FABD were changed to aspartic acid (CaMKIIβ-All D), completely lost F-actin binding activity, demonstrating that phosphorylation at the FABD is necessary and sufficient to prevent the interaction with F-actin. To test whether a similar mechanism was involved in migrating neurons, we electroporated the All D form of CaMKIIβ in the cerebral cortex as well as a phosphoblock All A mutant, where the same S and T residues were changed to alanine (CaMKIIβ-All A). While the All A mutant was as efficient as the wild-type to impair radial migration, the All D mutant did not induce any migration defect (Figures 5b and c). This result suggests that the detachment of CaMKIIβ from F-actin in migrating neurons is also controlled by phosphorylation sites in the FABD. Furthermore, since the migration defects were abolished with the All D mutant, which is unable to bind to actin, it further reinforces our previous result showing that an excessive binding of CaMKIIβ to the actin cytoskeleton induces migration defects in the developing cerebral cortex. These conclusions were strengthened by rescue experiments. Indeed, CaMKIIβ*-AllA was able to rescue the migration of *CaMKIIβ*-silenced neurons whereas CaMKIIβ*-AllD failed to counteract the migration acceleration seen upon *CaMKIIβ* depletion (Supplementary Figure 12). Taken together these data demonstrate that the phosphorylation sites in the F-actin binding domain control CaMKIIβ function in cortical neuron migration.

CaMKIIβ action in migrating neurons is tightly linked to cofilin activity

We next examined why an excessive actin binding impairs neuronal migration whereas *CaMKIIβ* silencing, and thus the absence of F-actin binding and crosslinking by CaMKIIβ, promotes migration. Interestingly, F-actin-CaMKIIβ interaction has been shown to limit access of actin-regulating proteins, like the actin depolymerizing cofilin, thereby inhibiting their actions and thus stabilizing F-actin structure 44. Inversely, the dissociation of CaMKIIβ from F-actin by autophosphorylation permits actin remodeling by actin-regulating proteins 44. In light of these data, we hypothesized that when we overexpressed CaMKIIβ, we prevented the interaction between cofilin and F-actin and consequently limited the activity of cofilin on actin. To counteract this effect of CaMKIIβ overexpression, we coelectroporated cofilinS3A, a nonphosphorylatable form of cofilin that continuously binds to actin filaments, or wild-type cofilin (cofilinWT). We found that cofilinS3A and cofilinWT are able to rescue the migration defects induced by CaMKIIβ overexpression, partially or totally respectively (Figures 6a-b). In accordance with our initial hypothesis, these data suggest that CaMKIIβ and cofilin competes for F-actin binding. In addition, the overexpression of CaMKIIβ decreased the G/F actin ratio in P19 cells (Figure 6c), which further suggest that CaMKIIβ overexpression might inhibit cofilin-induced actin depolymerization in nascent cortical neurons thus impairing their migration.

Inversely, we made the assumption that *CaMKIIβ* knockdown in migrating neurons favored the access of active cofilin (i.e. non phosphorylated form of cofilin) to F-actin. We thus tried to counteract this effect by overexpressing a phosphomimetic form of cofilin (cofilinS3D). Accordingly, overexpression of cofilinS3D fully rescued the migration of *CaMKIIβ*-silenced neurons (Supplementary Figures 13a-b). Moreover, because *CaMKIIβ* knockdown increased significantly the G/F actin ratio (Supplementary Figure 13c), our results suggest that *CaMKIIβ* silencing in cortical migrating neurons favors actin remodeling by cofilin, which might promote their movement. A precise balance between CaMKIIβ and cofilin activities is therefore required for proper migration of cortical neurons.

Discussion

In this study, we provide evidence that CaMKIIβ has an essential function in the development of the cerebral cortex. Indeed, we demonstrate that correct levels of CaMKIIβ are required for proper radial migration of projection neurons. In particular, CaMKIIβ controls the conversion between the multipolar and the bipolar stage as well as the step of locomotion in the CP, two actions which are dependent on its actin-binding and oligomerization domains.

CaMKIIβ regulates neuronal migration in the cerebral cortex: an isoform specific function

While CaMKIIα and β are the major brain isoforms, only the α isoform has been studied extensively, probably because of its prominent role in synaptic plasticity, learning, and memory 20, 21, 45–47. CaMKIIβ has often been relegated to a redundant role within heteromeric complexes or as a scaffold responsible for targeting CaMKII enzyme to F-actin in subcellular locations such as dendritic spines 24. Nevertheless, in systems where both CaMKIIα and β are present, CaMKIIβ has been shown to drive dendrite retraction and

pruning 27 and to regulate dendritic spine structure and synapse formation 28, 48. Here, we define a novel isoform-specific function for CaMKIIβ, in the absence of CaMKIIα, thus demonstrating that CaMKIIβ has a major biological function in the brain. Interestingly, γ and δ isoforms are also expressed in the developing cerebral cortex, especially in the VZ and CP 22. In addition, both γ and δ are able to bind to F-actin 49. While CaMKIIδ bundles actin filaments similarly to CaMKIIβ, γ isoform interaction with F-actin results in a completely different organization of filaments 49. Therefore, it will be interesting in future studies to determine whether CaMKIIγ and δ isoforms also contribute to corticogenesis and whether they have similar functions.

CaMKIIβ regulates migration through its action on the actin cytoskeleton

Our data obtained with the different mutants (Figure 4 and Supplementary Figure 10) suggest that CaMKIIβ regulates cortical neuronal migration independently of its kinase activity but through its actin-bundling activity. However we cannot totally exclude the involvement of CaMKIIβ kinase activity. Indeed, the experiment with the phospho-mutants (Figures 5b and c) suggests that the kinase activity of CaMKIIβ is required for FABD autophosphorylation and consequently for the detachment of CaMKIIβ from F-actin. Given this, the catalytically inactive mutant of CaMKIIβ (CaMKIIβ-K43R) might not be able to autophosphorylate FABD and detach from F-actin, thus inducing a more severe phenotype compared to wild-type CaMKIIβ. However, although not significant, migration defects after CaMKIIβ-K43R overexpression were somewhat less pronounced compared to CaMKIIβ wild-type overexpression. This might be due to the incapacity of CaMKIIβ-K43R to phosphorylate various proteins such as RhoGEFs or LIM-kinase, which ultimately leads to actin modification 50, 5152, 5351, 52. So CaMKIIβ might regulate the actin cytoskeleton in migrating neurons through kinase-dependent and independent activities.

Our data also indicate that CaMKIIβ impacts actin remodeling. However, it has been demonstrated previously that CaMKIIβ alone has no effect on actin polymerization/depolymerization 28, 44. Here we show that the action of CaMKIIβ is tightly linked to cofilin, an actin-depolymerizing protein also involved in the regulation cortical neuron migration 52, 53. The activity of cofilin on the actin cytoskeleton is well-known to be markedly altered by phosphorylation at serine 3 54. CofilinS3D, a phosphomimetic form of cofilin hence binds actin filaments with lower affinity than wild-type cofilin and weakly severs actin 55. Morever this mutant may act on endogenous cofilin in a dominant-negative manner, probably by competing for binding to phosphatases that dephosphorylate and thereby activate cofilin 56, 57. Inversely, cofilinS3A, a non phosphorylable form of cofilin, continuously bind to actin filaments and therefore functions as a constitutive active mutant. By using cofilinS3D and S3A mutants we were able to rescue the migration defects induced by *CaMKIIβ* knockdown or overexpression respectively thus demonstrating that a fine-tuned balance between CaMKIIβ and cofilin activities is necessary to ensure proper actin remodeling and migration of cortical neurons.

CaMKIIβ: a link between Ca^{2+} signaling and the actin cytoskeleton in cortical locomoting neurons

Locomotion is a saltatory, discontinuous process whereby neurons undergo periods of active movement interspersed by pauses. Interestingly, Ca^{2+} fluctuations have been described in the soma of migrating neurons during these different phases. More precisely, Rakic's group demonstrated that forward movement and stationary state during this process are tightly correlated with the peak and trough of Ca^{2+} fluctuation 58, 59. However as mentioned by the authors in their discussion "It is not well understood how transient elevations of $[Ca^{2+}]_i$ control the cell motility. One possibility is that fluctuations of $[Ca^{2+}]_i$ regulate the dynamic assembly and disassembly of cytoskeletal elements required for the operation of a force-generating mechanism involved in cell movement". In view of our data and those published in the literature, CaMKIIβ might be one of these elements mediating Ca^{2+} action on the cytoskeleton. Indeed, our data suggest that Ca^{2+} increase in locomoting neurons might dissociate CaMKIIβ from F-actin allowing actin remodeling by actin-modifying proteins such as cofilin and thus the forward movement. Inversely, when $[Ca^{2+}]_i$ decreases, CaMKIIβ might reassociate and bundle F-actin, this might limit access of actin-regulating proteins, thereby inhibiting their actions and stabilizing the actin cytoskeleton, which might lead to a pause. Interestingly, this cyclic regulation of CaMKIIβ and subsequently of the actin cytoskeleton organization by Ca^{2+} fluctuations has been recently described in spines, where CaMKIIβ acts as dynamic regulator of F-actin during synaptic plasticity 44.

Implications for neuropsychiatric and neurodevelopmental disorders

A series of recent studies indicate that CaMKII dysfunction is associated with a wide variety of psychiatric and neurodevelopmental diseases, including depression, schizophrenia, epilepsy and various forms of mental retardation 26, 60. Interestingly, among these studies, it was shown that CaMKIIβ expression is significantly elevated in frontal cortex of patients diagnosed with schizophrenia 25. In addition, an increase of CaMKIIβ expression was found in animal models of schizophrenia such as postnatal maternal deprivation and pubertal stress 61 as well as amphetamine sensitization 62. Here, our findings demonstrate that CaMKIIβ contributes to normal brain development by regulating the migration of cortical neurons and thus further support an important role for this gene in the pathophysiology of neurodevelopmental disorders. In view of these data and since abnormalities in neuronal migration are thought to cause brain disorders such as schizophrenia 2, it will be interesting to determine whether deregulation of CaMKIIβ contributes to the pathogenesis of this disease. Moreover because modification of CaMKIIβ expression is associated with multiple psychiatric illnesses 25, 63, 64, the identification of the upstream regulation of CaMKIIβ expression would provide a clue as to the original signal potentially leading to brain dysfunction. In conclusion, our study contributes to the understanding of cerebral cortex development and might provide insights into the physiopathology of multiple brain disorders.

Supplementary Material

Refer to Web version on PubMed Central for supplementary material.

Acknowledgments

We thank Dr Paul de Koninck for providing CaMKIIβ, Dr Azad Bonni for providing CaMKIIβ-ΔFABD, CaMKIIβ-Δasso, CaMKIIβ-K43R and CaMKIIβ-ΔCTS constructs, Dr Yasunori Hayashi for providing CaMKIIβ-All A and CaMKIIβ-All D. We are also grateful to Drs Iryna Ethell, Mary Hatten, Mathieu Vermeren and Franck Oury for providing the constructs expressing wild-type or mutated forms of cofilin, pCIG2-Centrin2-Venus, pCA-b-EGFPm5 silencer 3 and the RNA sens and antisense probes for *CaMKIIβ*, respectively. We gratefully acknowledge Dr Roberta Azzarelli for comments on the manuscript. Image analysis was partially done in the Bordeaux Imaging Center, a service unit of the CNRS-INSERM and Bordeaux University, member of the national infrastructure France BioImaging. This work benefited from the support of the Transcriptomic facility funded by INSERM and LabEX BRAIN ANR-10-LABX-43 and was supported by INSERM, CNRS, Bordeaux University, Marie Curie Actions (Intra European Fellowship), FRM (grant DEQ20130326468) and institutional funds from the Medical Research Council to F.G.

References

1. McManus MF, Golden JA. Neuronal migration in developmental disorders. Journal of child neurology. 2005; 20(4):280–286. [PubMed: 15921227]
2. Muraki K, Tanigaki K. Neuronal migration abnormalities and its possible implications for schizophrenia. Frontiers in neuroscience. 2015; 9:74. [PubMed: 25805966]
3. Stouffer MA, Golden JA, Francis F. Neuronal migration disorders: Focus on the cytoskeleton and epilepsy. Neurobiology of disease. 2015
4. Evsyukova I, Plestant C, Anton ES. Integrative mechanisms of oriented neuronal migration in the developing brain. Annual review of cell and developmental biology. 2013; 29:299–353.
5. Noctor SC, Martinez-Cerdeno V, Ivic L, Kriegstein AR. Cortical neurons arise in symmetric and asymmetric division zones and migrate through specific phases. Nature neuroscience. 2004; 7(2): 136–144. [PubMed: 14703572]
6. Kawauchi T. Cellullar insights into cerebral cortical development: focusing on the locomotion mode of neuronal migration. Frontiers in cellular neuroscience. 2015; 9:394. [PubMed: 26500496]
7. Bellion A, Baudoin JP, Alvarez C, Bornens M, Metin C. Nucleokinesis in tangentially migrating neurons comprises two alternating phases: forward migration of the Golgi/centrosome associated with centrosome splitting and myosin contraction at the rear. The Journal of neuroscience : the official journal of the Society for Neuroscience. 2005; 25(24):5691–5699. [PubMed: 15958735]
8. Schaar BT, McConnell SK. Cytoskeletal coordination during neuronal migration. Proceedings of the National Academy of Sciences of the United States of America. 2005; 102(38):13652–13657. [PubMed: 16174753]
9. Nadarajah B, Brunstrom JE, Grutzendler J, Wong RO, Pearlman AL. Two modes of radial migration in early development of the cerebral cortex. Nature neuroscience. 2001; 4(2):143–150. [PubMed: 11175874]
10. Heng JI, Chariot A, Nguyen L. Molecular layers underlying cytoskeletal remodelling during cortical development. Trends in neurosciences. 2010; 33(1):38–47. [PubMed: 19837469]
11. Kawauchi T, Hoshino M. Molecular pathways regulating cytoskeletal organization and morphological changes in migrating neurons. Developmental neuroscience. 2008; 30(1–3):36–46. [PubMed: 18075253]
12. Lian G, Sheen VL. Cytoskeletal proteins in cortical development and disease: actin associated proteins in periventricular heterotopia. Frontiers in cellular neuroscience. 2015; 9:99. [PubMed: 25883548]
13. Tsai LH, Gleeson JG. Nucleokinesis in neuronal migration. Neuron. 2005; 46(3):383–388. [PubMed: 15882636]
14. Yang T, Sun Y, Zhang F, Zhu Y, Shi L, Li H, et al. POSH localizes activated Rac1 to control the formation of cytoplasmic dilation of the leading process and neuronal migration. Cell reports. 2012; 2(3):640–651. [PubMed: 22959435]
15. Norden C, Young S, Link BA, Harris WA. Actomyosin is the main driver of interkinetic nuclear migration in the retina. Cell. 2009; 138(6):1195–1208. [PubMed: 19766571]

16. Solecki DJ, Trivedi N, Govek EE, Kerekes RA, Gleason SS, Hatten ME. Myosin II motors and F-actin dynamics drive the coordinated movement of the centrosome and soma during CNS glial-guided neuronal migration. Neuron. 2009; 63(1):63–80. [PubMed: 19607793]
17. Cooper JA. Molecules and mechanisms that regulate multipolar migration in the intermediate zone. Frontiers in cellular neuroscience. 2014; 8:386. [PubMed: 25452716]
18. Erondu NE, Kennedy MB. Regional distribution of type II Ca2+/calmodulin-dependent protein kinase in rat brain. The Journal of neuroscience: the official journal of the Society for Neuroscience. 1985; 5(12):3270–3277. [PubMed: 4078628]
19. Hell JW. CaMKII: claiming center stage in postsynaptic function and organization. Neuron. 2014; 81(2):249–265. [PubMed: 24462093]
20. Lisman J, Schulman H, Cline H. The molecular basis of CaMKII function in synaptic and behavioural memory. Nature reviews Neuroscience. 2002; 3(3):175–190. [PubMed: 11994750]
21. Wayman GA, Lee YS, Tokumitsu H, Silva AJ, Soderling TR. Calmodulin-kinases: modulators of neuronal development and plasticity. Neuron. 2008; 59(6):914–931. [PubMed: 18817731]
22. Bayer KU, Lohler J, Schulman H, Harbers K. Developmental expression of the CaM kinase II isoforms: ubiquitous gamma- and delta-CaM kinase II are the early isoforms and most abundant in the developing nervous system. Brain research Molecular brain research. 1999; 70(1):147–154. [PubMed: 10381553]
23. Lin YC, Redmond L. CaMKIIbeta binding to stable F-actin in vivo regulates F-actin filament stability. Proceedings of the National Academy of Sciences of the United States of America. 2008; 105(41):15791–15796. [PubMed: 18840684]
24. Shen K, Teruel MN, Subramanian K, Meyer T. CaMKIIbeta functions as an F-actin targeting module that localizes CaMKIIalpha/beta heterooligomers to dendritic spines. Neuron. 1998; 21(3): 593–606. [PubMed: 9768845]
25. Novak G, Seeman P, Tallerico T. Increased expression of calcium/calmodulin-dependent protein kinase IIbeta in frontal cortex in schizophrenia and depression. Synapse. 2006; 59(1):61–68. [PubMed: 16247765]
26. Robison AJ. Emerging role of CaMKII in neuropsychiatric disease. Trends in neurosciences. 2014; 37(11):653–662. [PubMed: 25087161]
27. Puram SV, Kim AH, Ikeuchi Y, Wilson-Grady JT, Merdes A, Gygi SP, et al. A CaMKIIbeta signaling pathway at the centrosome regulates dendrite patterning in the brain. Nature neuroscience. 2011; 14(8):973–983. [PubMed: 21725312]
28. Okamoto K, Narayanan R, Lee SH, Murata K, Hayashi Y. The role of CaMKII as an F-actin-bundling protein crucial for maintenance of dendritic spine structure. Proceedings of the National Academy of Sciences of the United States of America. 2007; 104(15):6418–6423. [PubMed: 17404223]
29. Pacary E, Heng J, Azzarelli R, Riou P, Castro D, Lebel-Potter M, et al. Proneural transcription factors regulate different steps of cortical neuron migration through Rndmediated inhibition of RhoA signaling. Neuron. 2011; 69(6):1069–1084. [PubMed: 21435554]
30. Pacary E, Guillemot F. Cerebral Cortex Electroporation to Study Projection Neuron Migration. Current protocols in neuroscience. 2016; 77:2 26 21–22 26 18. [PubMed: 27696363]
31. Pacary E, Haas MA, Wildner H, Azzarelli R, Bell DM, Abrous DN, et al. Visualization and genetic manipulation of dendrites and spines in the mouse cerebral cortex and hippocampus using in utero electroporation. Journal of visualized experiments : JoVE. 2012; (65)
32. Schneider CA, Rasband WS, Eliceiri KW. NIH Image to ImageJ: 25 years of image analysis. Nature methods. 2012; 9(7):671–675. [PubMed: 22930834]
33. Garcez PP, Diaz-Alonso J, Crespo-Enriquez I, Castro D, Bell D, Guillemot F. Cenpj/CPAP regulates progenitor divisions and neuronal migration in the cerebral cortex downstream of Ascl1. Nature communications. 2015; 6:6474.
34. Schindelin J, Arganda-Carreras I, Frise E, Kaynig V, Longair M, Pietzsch T, et al. Fiji: an open-source platform for biological-image analysis. Nature methods. 2012; 9(7):676–682. [PubMed: 22743772]

35. Azzarelli R, Pacary E, Garg R, Garcez P, van den Berg D, Riou P, et al. An antagonistic interaction between PlexinB2 and Rnd3 controls RhoA activity and cortical neuron migration. Nature communications. 2014; 5:3405.
36. Oury F, Yadav VK, Wang Y, Zhou B, Liu XS, Guo XE, et al. CREB mediates brain serotonin regulation of bone mass through its expression in ventromedial hypothalamic neurons. Genes & development. 2010; 24(20):2330–2342. [PubMed: 20952540]
37. Fulga TA, Elson-Schwab I, Khurana V, Steinhilb ML, Spires TL, Hyman BT, et al. Abnormal bundling and accumulation of F-actin mediates tau-induced neuronal degeneration in vivo. Nat Cell Biol. 2007; 9(2):139–148. [PubMed: 17187063]
38. Fajol A, Honisch S, Zhang B, Schmidt S, Alkahtani S, Alarifi S, et al. Fibroblast growth factor (Fgf) 23 gene transcription depends on actin cytoskeleton reorganization. FEBS letters. 2016; 590(6):705–715. [PubMed: 26878191]
39. Bustin SA, Benes V, Garson JA, Hellemans J, Huggett J, Kubista M, et al. The MIQE guidelines: minimum information for publication of quantitative real-time PCR experiments. Clinical chemistry. 2009; 55(4):611–622. [PubMed: 19246619]
40. Livak KJ, Schmittgen TD. Analysis of relative gene expression data using real-time quantitative PCR and the 2(-Delta Delta C(T)) Method. Methods. 2001; 25(4):402–408. [PubMed: 11846609]
41. Nichols AJ, Carney LH, Olson EC. Comparison of slow and fast neocortical neuron migration using a new in vitro model. BMC neuroscience. 2008; 9:50. [PubMed: 18534012]
42. Insolera R, Shao W, Airik R, Hildebrandt F, Shi SH. SDCCAG8 regulates pericentriolar material recruitment and neuronal migration in the developing cortex. Neuron. 2014; 83(4):805–822. [PubMed: 25088364]
43. Shen K, Meyer T. Dynamic control of CaMKII translocation and localization in hippocampal neurons by NMDA receptor stimulation. Science. 1999; 284(5411):162–166. [PubMed: 10102820]
44. Kim K, Lakhanpal G, Lu HE, Khan M, Suzuki A, Hayashi MK, et al. A Temporary Gating of Actin Remodeling during Synaptic Plasticity Consists of the Interplay between the Kinase and Structural Functions of CaMKII. Neuron. 2015; 87(4):813–826. [PubMed: 26291163]
45. Giese KP, Fedorov NB, Filipkowski RK, Silva AJ. Autophosphorylation at Thr286 of the alpha calcium-calmodulin kinase II in LTP and learning. Science. 1998; 279(5352):870–873. [PubMed: 9452388]
46. Malinow R, Schulman H, Tsien RW. Inhibition of postsynaptic PKC or CaMKII blocks induction but not expression of LTP. Science. 1989; 245(4920):862–866. [PubMed: 2549638]
47. Silva AJ, Stevens CF, Tonegawa S, Wang Y. Deficient hippocampal long-term potentiation in alpha-calcium-calmodulin kinase II mutant mice. Science. 1992; 257(5067):201–206. [PubMed: 1378648]
48. Fink CC, Bayer KU, Myers JW, Ferrell JE Jr, Schulman H, Meyer T. Selective regulation of neurite extension and synapse formation by the beta but not the alpha isoform of CaMKII. Neuron. 2003; 39(2):283–297. [PubMed: 12873385]
49. Hoffman L, Farley MM, Waxham MN. Calcium-calmodulin-dependent protein kinase II isoforms differentially impact the dynamics and structure of the actin cytoskeleton. Biochemistry. 2013; 52(7):1198–1207. [PubMed: 23343535]
50. Saneyoshi T, Hayashi Y. The Ca2+ and Rho GTPase signaling pathways underlying activity-dependent actin remodeling at dendritic spines. Cytoskeleton. 2012; 69(8):545–554. [PubMed: 22566410]
51. Saito A, Miyajima K, Akatsuka J, Kondo H, Mashiko T, Kiuchi T, et al. CaMKIIbetamediated LIM-kinase activation plays a crucial role in BDNF-induced neuritogenesis. Genes to cells : devoted to molecular & cellular mechanisms. 2013; 18(7):533–543. [PubMed: 23600483]
52. Chai X, Zhao S, Fan L, Zhang W, Lu X, Shao H, et al. Reelin and cofilin cooperate during the migration of cortical neurons: a quantitative morphological analysis. Development. 2016; 143(6): 1029–1040. [PubMed: 26893343]
53. Kawauchi T, Chihama K, Nabeshima Y, Hoshino M. Cdk5 phosphorylates and stabilizes p27kip1 contributing to actin organization and cortical neuronal migration. Nature cell biology. 2006; 8(1): 17–26. [PubMed: 16341208]

54. Nagaoka R, Abe H, Obinata T. Site-directed mutagenesis of the phosphorylation site of cofilin: its role in cofilin-actin interaction and cytoplasmic localization. Cell motility and the cytoskeleton. 1996; 35(3):200–209. [PubMed: 8913641]
55. Elam WA, Cao W, Kang H, Huehn A, Hocky GM, Prochniewicz E, et al. Phosphomimetic S3D-Cofilin Binds But Only Weakly Severs Actin Filaments. The Journal of biological chemistry. 2017
56. Shi Y, Pontrello CG, DeFea KA, Reichardt LF, Ethell IM. Focal adhesion kinase acts downstream of EphB receptors to maintain mature dendritic spines by regulating cofilin activity. The Journal of neuroscience : the official journal of the Society for Neuroscience. 2009; 29(25):8129–8142. [PubMed: 19553453]
57. Uenishi E, Shibasaki T, Takahashi H, Seki C, Hamaguchi H, Yasuda T, et al. Actin dynamics regulated by the balance of neuronal Wiskott-Aldrich syndrome protein (N-WASP) and cofilin activities determines the biphasic response of glucose-induced insulin secretion. The Journal of biological chemistry. 2013; 288(36):25851–25864. [PubMed: 23867458]
58. Komuro H, Rakic P. Intracellular Ca2+ fluctuations modulate the rate of neuronal migration. Neuron. 1996; 17(2):275–285. [PubMed: 8780651]
59. Rash BG, Ackman JB, Rakic P. Bidirectional radial Ca(2+) activity regulates neurogenesis and migration during early cortical column formation. Science advances. 2016; 2(2):e1501733. [PubMed: 26933693]
60. Ma H, Groth RD, Cohen SM, Emery JF, Li B, Hoedt E, et al. gammaCaMKII shuttles Ca(2)(+)/CaM to the nucleus to trigger CREB phosphorylation and gene expression. Cell. 2014; 159(2): 281–294. [PubMed: 25303525]
61. Novak G, Fan T, O'Dowd BF, George SR. Postnatal maternal deprivation and pubertal stress have additive effects on dopamine D2 receptor and CaMKII beta expression in the striatum. International journal of developmental neuroscience : the official journal of the International Society for Developmental Neuroscience. 2013; 31(3):189–195. [PubMed: 23313435]
62. Greenstein R, Novak G, Seeman P. Amphetamine sensitization elevates CaMKIIbeta mRNA. Synapse. 2007; 61(10):827–834. [PubMed: 17603807]
63. Li K, Zhou T, Liao L, Yang Z, Wong C, Henn F, et al. betaCaMKII in lateral habenula mediates core symptoms of depression. Science. 2013; 341(6149):1016–1020. [PubMed: 23990563]
64. Voineagu I, Wang X, Johnston P, Lowe JK, Tian Y, Horvath S, et al. Transcriptomic analysis of autistic brain reveals convergent molecular pathology. Nature. 2011; 474(7351):380–384. [PubMed: 21614001]

Europe PMC Funders Author Manuscripts

Europe PMC Funders Author Manuscripts

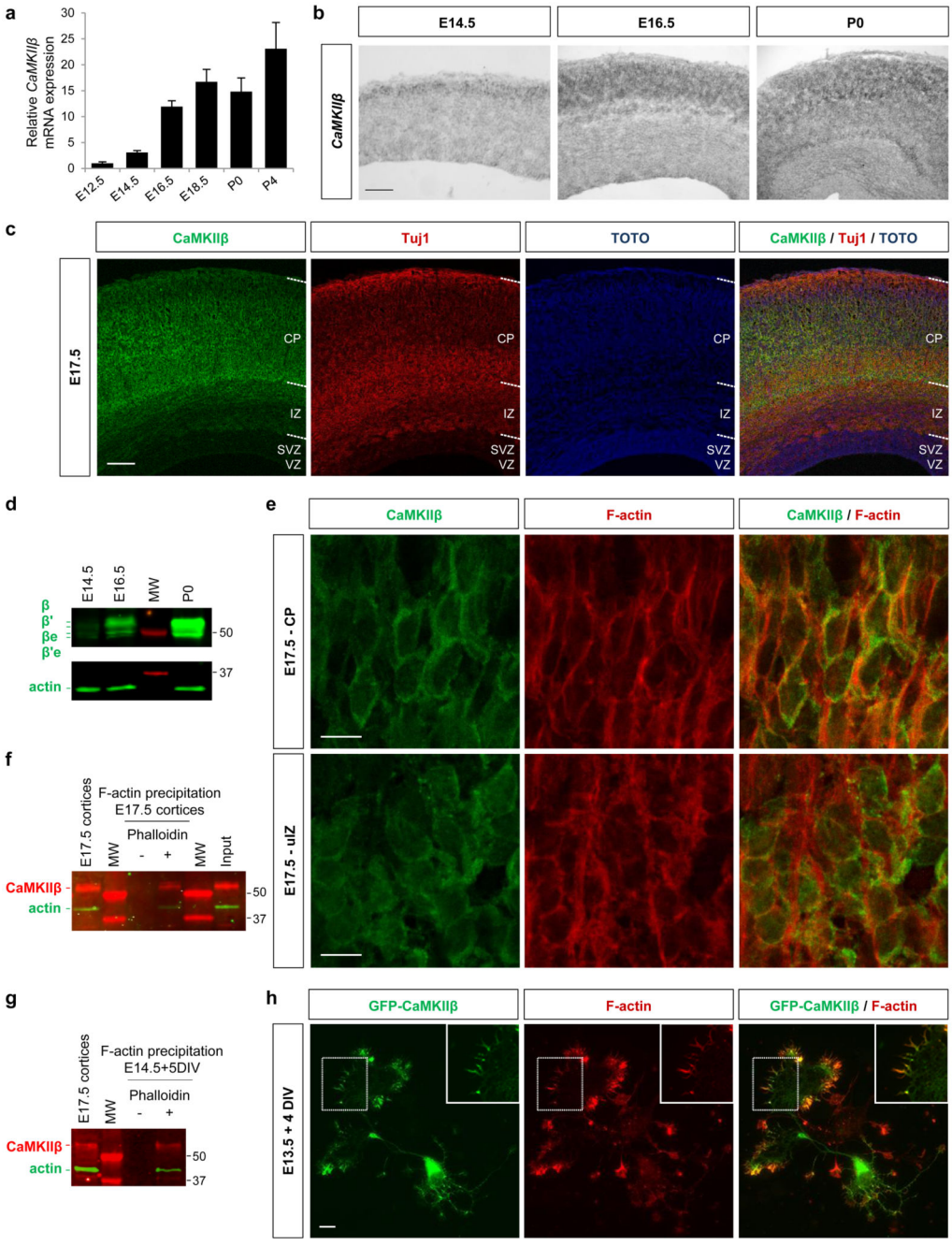

Figure 1. CaMKIIβ is expressed in the developing cerebral cortex and interacts with F-actin in cortical neurons.

(**a**) Analysis by real-time PCR of *CaMKIIβ* mRNA expression in the developing cerebral cortex. Data are presented as fold change compared to the expression level at E12.5 ± s.e.m. (n=3-5 embryos). (**b**) Distribution of *CaMKIIβ* transcripts in coronal sections of the developing cerebral cortex at E14.5, E16.5, and P0. (**c**) E17.5 coronal cortical sections immunostained for CaMKIIβ (green) and the postmitotic neuronal marker Tuj1 (red). Nuclei were labelled with TOTO. VZ, ventricular zone; SVZ, subventricular zone; IZ,

intermediate zone; CP, cortical plate. (**d**) CaMKIIβ and actin immunoblotting analyses of lysates from E14.5, E16.5, and P0 cortices. Molecular weight (MW) in kDa is indicated in all blots. Full-length blots are presented in Supplementary Figure 14. (**e**) Immunostaining for CaMKIIβ (green) and F-actin (red) in the CP and upper intermediate zone (uIZ) at E17.5. (**f**) Precipitation of F-actin from E17.5 cerebral cortices using biotinylated phalloidin and immunoblotting of the precipitated material with CaMKIIβ and actin antibodies. Representative image of three independent experiments. (**g**) F-actin from neuronal cell cultures was precipited using biotinylated phalloidin and the precipitated materiel as well as E17.5 cerebral cortex extracts were probed for CaMKIIβ and actin. (**h**) Cortical neuron cultures transfected with GFP-CaMKIIβ (CaMKIIβ cloned into the pEGFP-C1 vector) and stained with rhodamine-labelled phalloidin to visualize F-actin. White rectangles show areas enlarged in the insets. Representative image of three independent experiments.
Scale bars represent 100 μm (b, c) and 10 μm (e, h).
See also Supplementary Figure 1.

Europe PMC Funders Author Manuscripts

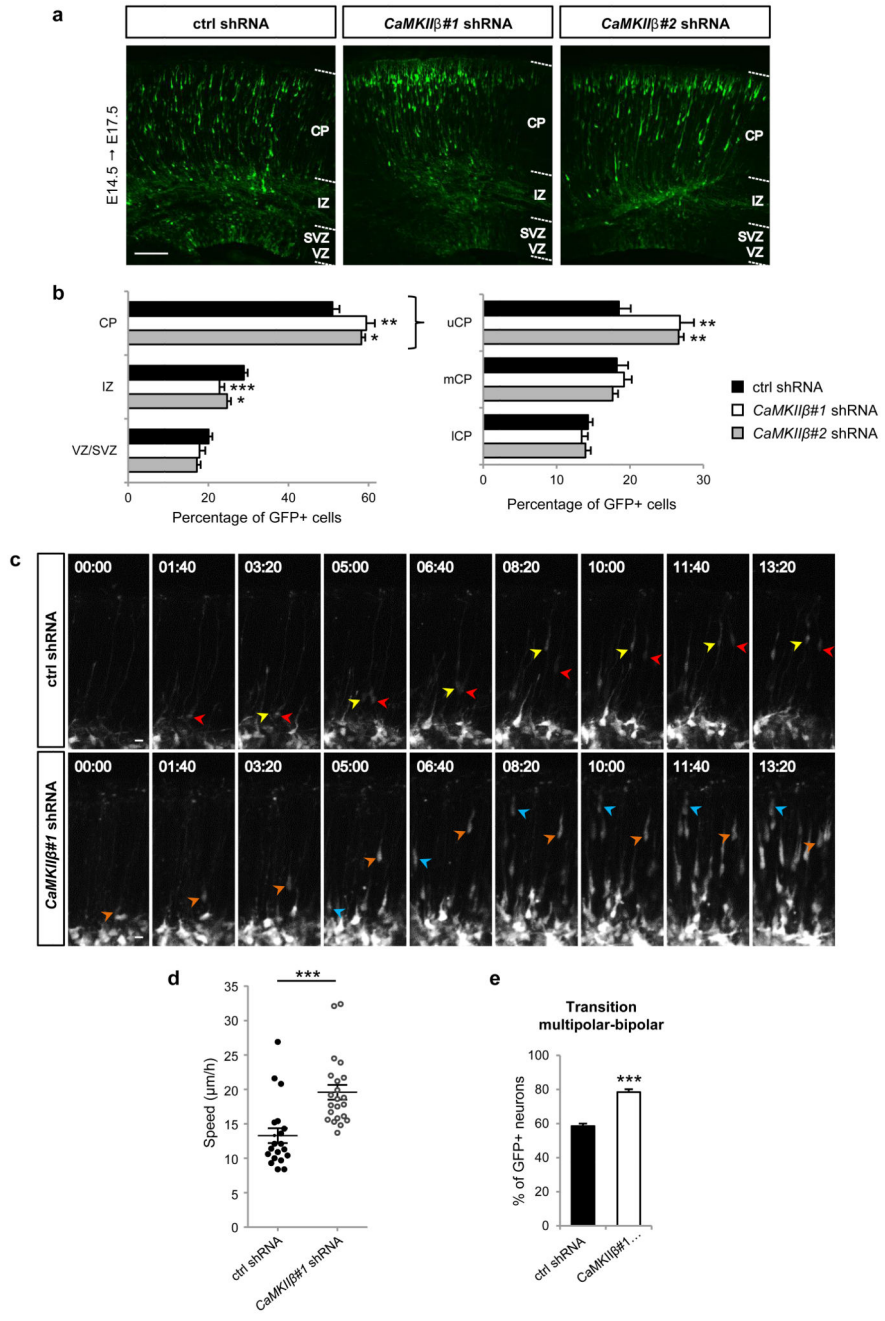

Figure 2. CaMKIIβ knockdown promotes radial migration of projection neurons in the cerebral cortex.

(**a**) Representative images of E17.5 cortices electroporated with control (ctrl) shRNA, *CaMKIIβ#1* shRNA or *CaMKIIβ#2* shRNA at E14.5. (**b**) The quantification graph shows the distribution of electroporated (GFP^+) cells in different zones of the cortex in the different electroporation experiments. The CP is further subdivided into upper CP (uCP), median CP (mCP) and lower CP (lCP). Data are presented as the mean ± s.e.m. from at least seven sections prepared from at least four embryos obtained from two litters. Similar experimental

design and quantification were used in subsequent experiments. One-way ANOVA followed by a Fisher's PLSD post hoc test; *p < 0.05, **p < 0.01, ***p < 0.001 compared to ctrl shRNA. (**c**) Time-lapse series of GFP+ cells located into the CP after electroporation (E14.5) of ctrl or *CaMKIIβ#1* shRNA. Yellow and red arrowheads point control cells, orange and blue arrowheads point *CaMKIIβ#1* silenced cells. Time is depicted in hours and minutes. (**d**) Quantification of individual and averaged migration speed from 20 control cells and 22 *CaMKIIβ#1* silenced cells obtained in each condition from 3 different sections prepared from 3 embryos obtained from two litters. Mean ± s.e.m.; unpaired two-tailed Student's t-test; ***p < 0.001. **(e)** Percentage of electroporated neurons exhibiting multipolar-bipolar conversion during 10 hour recording. Mean ± s.e.m.; unpaired two-tailed Student's t-test; ***p < 0.001.

Scale bars represent 100 μm (a) and 10 μm (c).

See also Supplementary Figures 2-6 and Supplementary Movies 1-4.

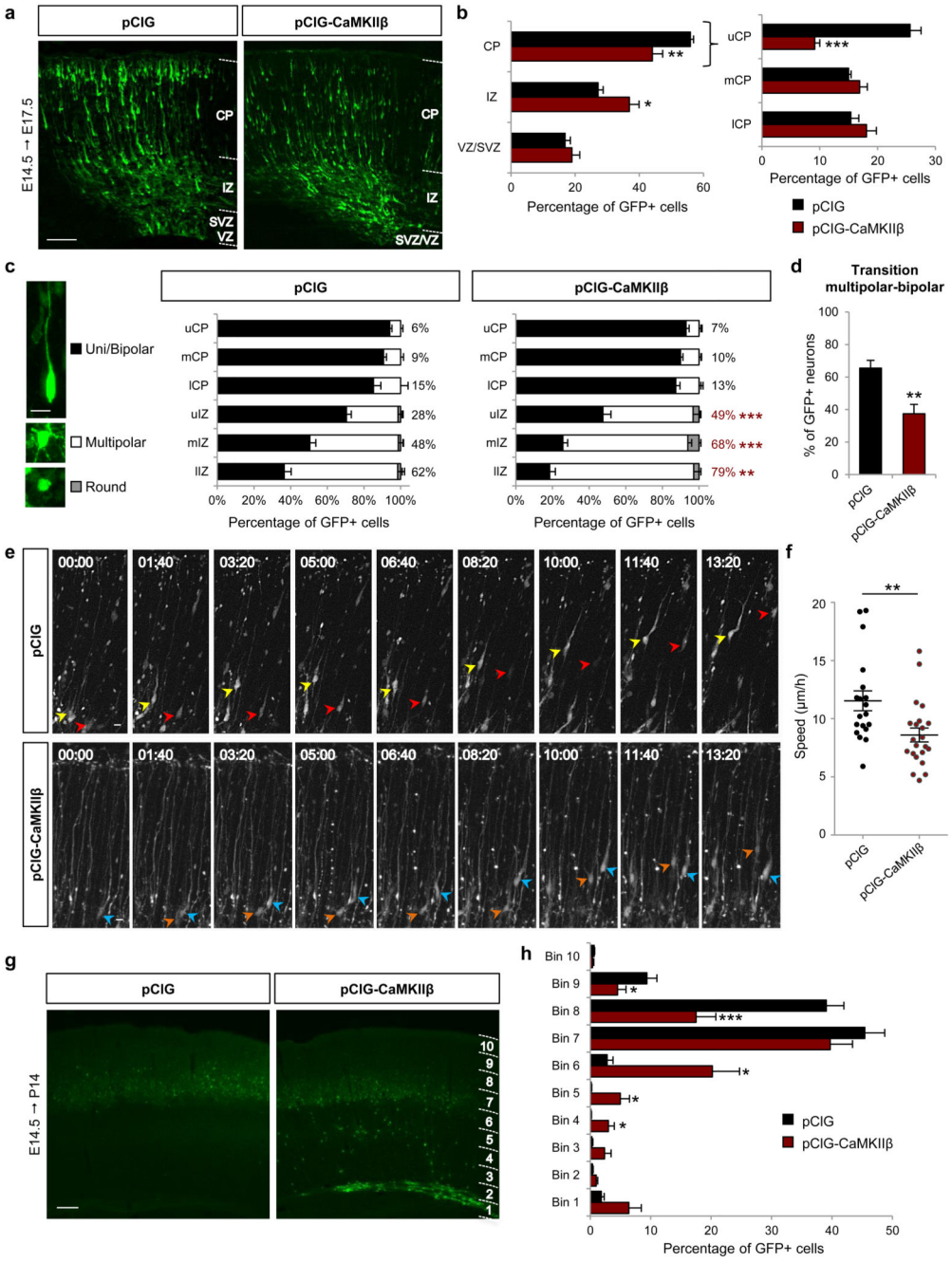

Figure 3. Overexpression of CaMKIIβ alters migration of cortical projection neurons.

(**a**) Representative images of E17.5 cortices electroporated with a control plasmid (pCIG panel) or a plasmid expressing CaMKIIβ under the CAG promoter (pCIG-CaMKIIβ panel) together with a GFP vector at E14.5. (**b**) Quantification of the distribution of GFP^+ cells in the cortex at E17.5. Mean ± s.e.m.; unpaired two-tailed Student's t-test; *p < 0.05, **p < 0.01, ***p < 0.001. (**c**) Quantification of the morphology of electroporated cells in the different zones of the cortex. The percentages represent the proportion of multipolar cells in each zone. Pictures illustrate the different morphologies of migrating projection neurons.

Data are presented as the mean ± s.e.m. from at least six sections prepared from at least three embryos obtained from two or three litters (more than 1500 cells were analyzed in each condition); unpaired two-tailed Student's t-test; **p < 0.01, ***p < 0.001 compared to pCIG. (**d**) Percentage of electroporated neurons exhibiting multipolar-bipolar conversion during 10 hour recording. Mean ± s.e.m.; unpaired two-tailed Student's t-test; **p < 0.01. (**e**) Time-lapse series of GFP+ cells located into the CP after electroporation (E14.5) of pCIG or pCIG-CaMKIIβ. Yellow and red arrowheads point control cells, orange and blue arrowheads point *CaMKIIβ* overexpressing cells. Time is depicted in hours and minutes. (**f**) Quantification of individual and averaged migration speed from 19 control cells and 22 *CaMKIIβ* expressing cells obtained in each condition from 3 different sections prepared from 3 embryos obtained from two litters. Mean ± s.e.m.; unpaired two-tailed Student's t-test; **p < 0.01. (**g**, **h**) Distribution of GFP^+ cells at P14 in the cortex divided into 10 bins after pCIG or pCIG-CaMKIIβ electroporation at E14.5. Mean ± s.e.m.; Unpaired two-tailed Student's t-test; *p < 0.05, ***p < 0.001.

Scale bars represent 100 μm (a, g) and 10 μm (c, e).

See also Supplementary Figures 7-9 and Supplementary Movies 5-8.

Europe PMC Funders Author Manuscripts

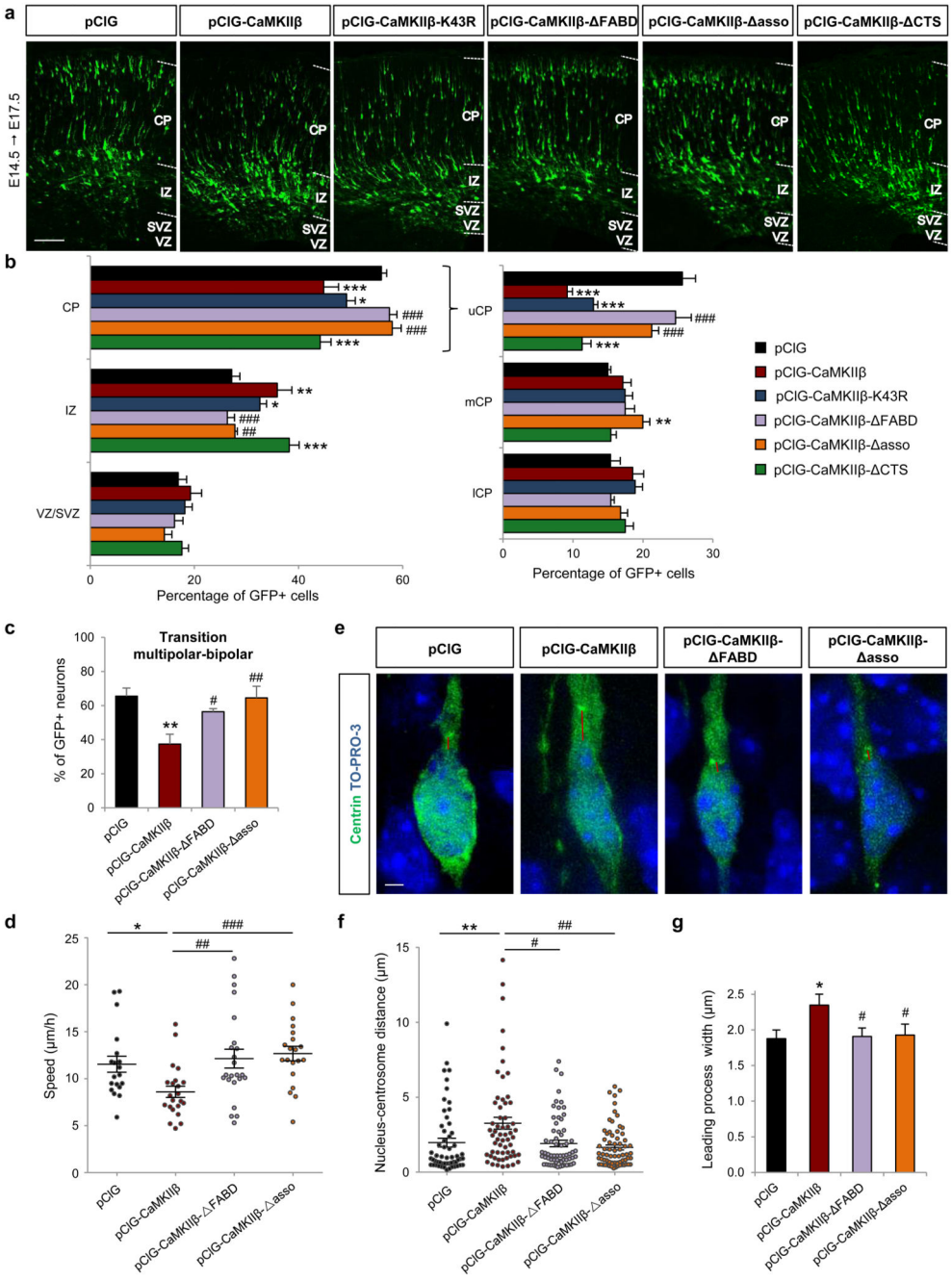

Figure 4. CaMKIIβ regulates neuronal migration through its actin-bundling activity.

(**a**) Representative images of E17.5 cortices electroporated with a control plasmid, a plasmid expressing wild-type CaMKIIβ or a catalytically inactive mutant of CaMKIIβ in which the ATP binding site was disrupted (K43R) or a mutated form of CaMKIIβ without F-actin binding domain (ΔFABD) or a mutated form without the association domain (Δasso) or a mutated form without the centrosomal targeting sequence (ΔCTS), together with GFP at E14.5. (**b**) Graphs show the distribution of electroporated GFP^+ cells per cortical compartment in the different conditions. Mean ± s.e.m.; One-way ANOVA followed by a

Fisher's PLSD post hoc test; *p < 0.05, **p < 0.01, ***p < 0.001 compared to pCIG condition; ##p < 0.01, ###p < 0.001 compared to pCIG-CaMKIIβ condition. (**c**) Percentage of GFP+ neurons exhibiting multipolar-bipolar conversion during 10 hour recording after electroporation with the indicated constructs. Mean ± s.e.m.; One-way ANOVA followed by a Fisher's PLSD post hoc test; **p < 0.01 compared to pCIG; #p < 0.05 and ##p < 0.01 compared to pCIG-CaMKIIβ. (**d**) Quantification of individual and averaged migration speed from 19 control cells, 22 *CaMKIIβ* expressing cells, 23 ΔFABD and 20 Δasso expressing cells obtained in each condition from 3 different sections prepared from 3 embryos obtained from two litters. Mean ± s.e.m.; One-way ANOVA followed by a Fisher's PLSD post hoc test; *p < 0.05 compared to pCIG; ##p < 0.01, ###p < 0.001 compared to pCIG-CaMKIIβ. (**e-f**) Analysis at E17.5 of the distance (depicted by a red line) between the centrosome and the tip of the nucleus in cortical neurons electroporated 3 days before with the indicated constructs together with pCIG2-Centrin2-Venus. The nucleus was labelled with TO-PRO-3. Mean ± s.e.m.; n=56 cells for pCIG, n=59 cells for pCIG-CaMKIIβ, n=65 cells for pCIG-CaMKIIβ-ΔFABD, n=70 cells for pCIG-CaMKIIβ-Δasso from at least three embryos obtained from two litters; Kruskal-Wallis test followed by Dunn's multiple comparison test. **p < 0.01 compared to pCIG condition; #p < 0.05, ##p < 0.01 compared to pClG-CaMKIIβ condition. (**g**) Quantification of the leading process width in cortical neurons electroporated 3 days before with the indicated constructs. Mean ± s.e.m.; n=41 cells for pCIG, n=50 cells for pCIG-CaMKIIβ, n=53 cells for pCIG-CaMKIIβ-ΔFABD, n=56 cells for pCIG-CaMKIIβ-Δasso from at least three embryos obtained from two litters; One-way ANOVA followed by a Fisher's PLSD post hoc test; *p < 0.05 compared to pCIG condition; ##p < 0.01 compared to pCIG-CaMKIIβ condition.

Scale bars represent 100 μm (a) and 2 μm (e).

See also Supplementary Figures 10 and 11.

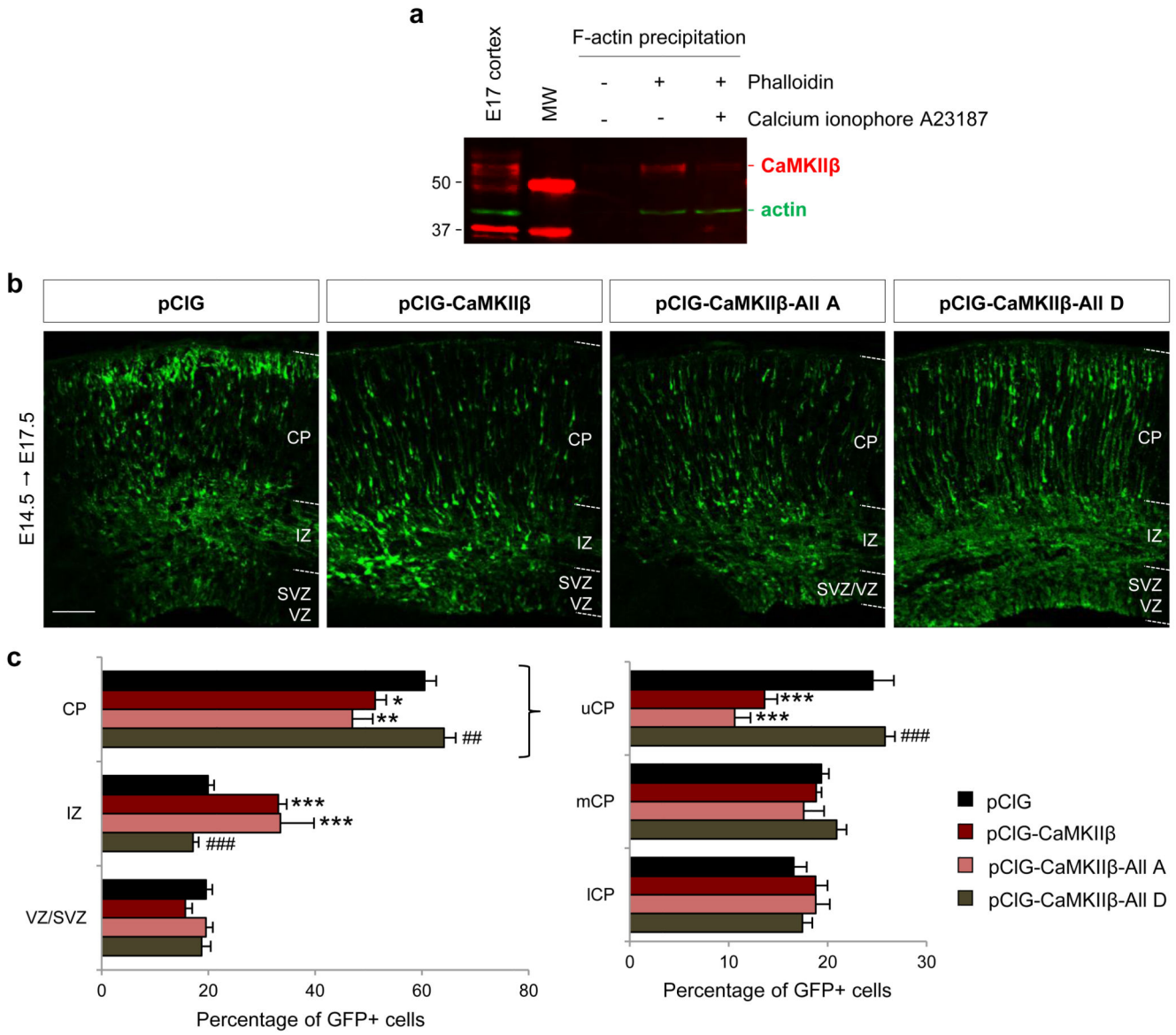

Figure 5. Autophosphorylation sites within the FABD control CaMKIIβ action in migrating neurons

(**a**) F-actin from neuronal cell cultures treated or not with the calcium ionophore A23187 was precipited using biotinylated phalloidin and the precipitated materiel as wells as E17.5 cerebral cortex extracts were probed for CaMKIIβ and actin. Representative image of three independent experiments. (**b**) Representative images of E17.5 cortices electroporated with a control plasmid, a plasmid expressing wild-type CaMKIIβ or a nonphosphorylatable form of CaMKIIβ (All A) or a phosphomimetic All D mutant, together with a GFP vector at E14.5. (**c**) Graphs show the distribution of electroporated GFP+ cells per cortical compartment in the different conditions. Mean ± s.e.m.; One-way ANOVA followed by a Fisher's PLSD post hoc test; *p < 0.05, **p < 0.01, ***p < 0.001 compared to pCIG condition; ###p < 0.001 compared to pCIG-CaMKIIβ condition.

Scale bar represents 100 μm (b).

Europe PMC Funders Author Manuscripts

See also Supplementary Figure 12.

Europe PMC Funders Author Manuscripts

Europe PMC Funders Author Manuscripts

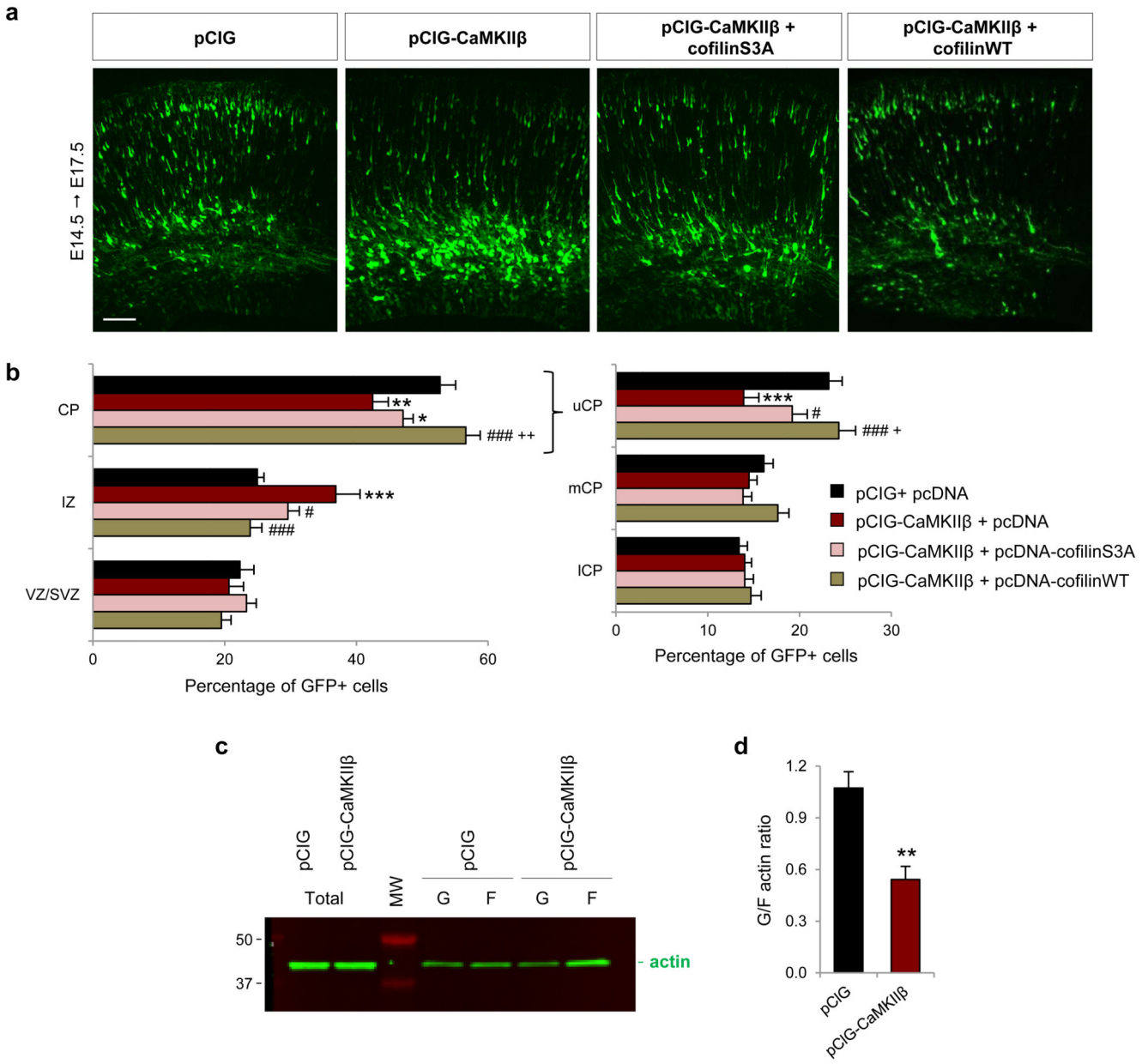

Figure 6. CaMKIIβ inhibits cofilin-F-actin interaction and affects actin dynamics.

(**a**) Representative images of E17.5 cortices electroporated at E14.5 with the indicated constructs. (**b**) Graphs show the distribution of electroporated GFP^+ cells per cortical compartment in the different conditions. Mean ± s.e.m.; One-way ANOVA followed by a Fisher's PLSD post hoc test; *p < 0.05, **p < 0.01, ***p < 0.001 compared to pCIG; #p < 0.05, ###p < 0.001 compared to pCIG-CaMKIIβ; +p < 0.05, ++p<0.01 compared to pCIG-CaMKIIβ + pcDNA-cofilinS3A. (**c**) Western blot of total, G- and F-actin fractions from P19 cells transfected for 24 h with CaMKIIβ overexpressing or control constructs and (**d**) quantification of the G/F actin ratio from 4 independent experiments. Mean ± s.e.m.; unpaired two-tailed Student's t-test; **p < 0.01.

Scale bar represents 100 μm (a).

See also Supplementary Figure 13.

Europe PMC Funders Author Manuscripts

Europe PMC Funders Author Manuscripts

Table 1

Sequences of primers used for qPCR.

Gene	GenBank ID	Forward Sequence (5'-3')	Reverse Sequence (5'-3')
CaMKIIα	AW490258	GTGCCTTGACCAATTCAGGAA	TTGGCGTTTTCAGTGGAATAAA
CaMKIIβ	NM_001174053	TGGCCAGTGCTGTAGTGTGTTAC	GGAACTCAGCAAAAAGAGAGAAGAG
CaMKIIδ	NM_001025439	AGGCCGGAGCTTACGATTTT	TTGATGAGGTCTTTGGCTTCAG
CaMKIIγ	NM_178597	TGGGCTGCCTCCCTTCTT	AGCAGTCAGTTCGATCTCAAACC
β variant	NM_007595	ACCGCTCCGGCCACAATGT	TGGATAACGGTGGTTTGAGGC
β' variant	NM_007595	ACCGCTCCGGCCACAATGT	TGCTGTCGGAAGATTCCAGG
βe variant	NM_001174054	ACACGGAATTTCTCAGCAGCC	GCAGGAGGGAGAGATCCTTT
β'e variant	NM_001174053	CACACGGAATTTCTCAGCCAA	GCAGGAGGGAGAGATCCTTT